Double Diffusive Effects in Buoyancy Driven Exchange Flow of Miscible Fluids in Inclined Pipes

A Thesis

Presented to

The Faculty of the Department of Mechanical Engineering

University of Houston

In Partial Fulfillment

of the Requirement of the Degree

Master of Science

in

Mechanical Engineering

By

Shadi Shariatnia

December 2016

Double Diffusive Effects in Buoyancy Driven Exchange Flow of Miscible Fluids in Inclined Pipes

Shadi Shariatnia

Approved:

Chair of Committee
Hadi Ghasemi, Assistant Professor
Mechanical Engineering

Committee Members:

Ralph Metcalfe, Professor
Mechanical Engineering

Kamran Alba, Assistant Professor
College of Technology

Suresh K. Khator, Associate Dean
Cullen College of Engineering

Pradeep Sharma, Professor and Chair
Mechanical Engineering

Acknowledgment

Fisrt of all, I would like to express my sincere gratitude to my advisors, Professor Ghasemi and Alba for their patience, guidance and support during my Masters program. I learnt so much from their knowledge and critical thinking. I could not have imagined having better mentors.

In the committee I would like to thank Professor Metcalfe for responding all my questions with patience and accepting to be in my thesis committee. His comments during this project advanced my research.

I would also like to thank University of Houston for supporting this project and my colleagues, specifically Bahare Eslami, in ComplexFluids Lab for their help in different stages of this study.

I am grateful to all my friends who have always motivated me, specially Hessam Mohammadmoradi helped me a lot with programming parts of my project. I learnt a lot from his humble knowledge.

Finally, the greatest gratitude goes to my family, my mother, father and sister for their constant love, encouragement and support. I wouldn't be here if it wasn't for them.

Double Diffusive Effects in Buoyancy Driven Exchange Flow of Miscible Fluids in Inclined Pipes

A Thesis

Presented to

The Faculty of the Department of Mechanical Engineering

University of Houston

In Partial Fulfillment

of the Requirement of the Degree

Master of Science

in

Mechanical Engineering

By

Shadi Shariatnia

December 2016

Abstract

We study double diffusion buoyancy-driven exchange flow of two miscible Newtonian fluids in an inclined pipe experimentally. Experiments have been carried in an adiabatic small-aspect-ratio pipe and the fluids involved are isoviscous. Inclined configuration has been studied for the first time in this research. There has also been observed a novel asymmetric behavior in the flow which has never been observed before in the isothermal limit in which the cold finger appears to advance faster than the hot one. complementary experiments have been done to clarify this asymmetric behavior is associated with the wall contact and the formation of a warm less-viscous film of the fluid lubricating the cold more-viscous finger along the pipe. On the other side of the pipe, a cool more-viscous film forms decelerating the hot less-viscous finger. The asymmetric behavior of the flow is finally quantified over the full range of experiments carried.

Table of Contents

List of Figures

List of Tables

1 Introduction

1.1 Theoretical Basis

Buoyancy-driven exchange flow of two miscible fluids due to the interpenetration of a dense fluid into a light one has significant importance in fluid dynamics contexts. These flows are abundantly found in nature, in oceanographic, meteorological and geophysical contexts [1-3], and also play an important role in industry. From exchange flows applications in continuous reactors [6, 7], and well cementing [8] to Counter-Current Extraction Columns (CCEC), Which themselves have wide range of applications in other industries, such as food and beverage (distilled alcoholic drinks extracts production [4], supercritical Co_2 extraction [5], etc. Due to certain process constraints, inclined columns may be preferred over the vertical ones [8-11]. Isothermal exchange flows in which both fluids have same temperature and density difference comes from other resources (such as adding salinity) have been studied in literature experimentally [15-18], computationally [19-21] and analytically [22, 23] to a great extent.

The fluids involved in exchange flows may generally contain both temperature and salinity gradients. The heat and mass in such systems can diffuse at different rates causing the emergence of fascinating *Double Diffusive (DD)* effects, which are widely found in nature in oceans [29], magma chambers [30], lava fingers [31] and solar planet interiors [32] as well as industry [33-35]. Depending on the fluids stratification, DD convection in a vertically-layered two-fluid system can be either in *diffusive* and/or *finger* mode [29]. In diffusive-type DD convection, a series of horizontal diffuse layers form at different depths with convective rolls moving in between the layers [36]. The thickness of these diffuse layers increases with temperature difference and decreases with the initial concentration

difference [37]. On the other hand, the finger-type DD convection is characterized by exponentially growing long thin fingers interpenetrating down through the medium and, conversely, fresh fingers moving upward [36]. The DD effects can also play a major role when the temperature and salinity gradients are imposed laterally [38-41]. Depending on the flow configuration, one may face *aiding* and/or *opposing* buoyancy forces which affect the thermal and concentration fronts [42]. Steady multi-cell structures are found at larger Lewis numbers (thermal to mass diffusivity ratio) experimentally [38, 39] and numerically [40]. Similar duplicated flow patterns can be observed as the lateral aspect ratio increases, which can drastically affect the rates of heat and mass transfer [43]. So far, the intriguing DD effects have only been studied in depth for purely vertical [29-31, 36, 37, 44-51] and/or horizontal [38-43] configurations. We aim to study such a fundamental problem in an inclined geometry prevalent in nature and industry.

Vertical [12] and inclined [13-16] tubes have been studied in the case of isothermal buoyancy driven exchange flows and different flow regimes have been observed based on different flow parameters. These regimes have been classified as viscous, transitionary and diffusive flows. As tilting angle changes from horizontal to vertical, interfacial instabilities and counter current flows (Kelvin-Helmholtz instability) [24, 25] increase and also due to density gradients (Rayleigh-Taylor instability) [26] and viscosity gradient [27, 28] flow has a transition from viscous, at low inclination angles, to fully diffusive configuration, at high tilt angles [15]. At the beginning of the buoyant exchange flow there is a buoyant-inertial force balance which changes to buoyant-viscous balance as the heavy fluid interpenetrates in the light one. The transition happens at $Re_t Cos\beta \geq 50$, where $Re_t = \frac{\hat{V}_v}{\hat{V}_t}$ is a critical Reynolds number with $V_v = \frac{At\, \hat{g}\, \hat{D}^2}{\nu}$ and $V_t = (At\, \hat{g}\, \hat{D}\,)^{1/2}$, where $\hat{\rho}$, $\hat{\mu}$, $\hat{g}$, and

$At = \frac{\rho_H - \rho_L}{\rho_H + \rho_L}$, are the average density, average viscosity, gravitational acceleration and the Atwood number characterizing the density difference between the heavy and light fluids, respectively. Propagating front velocity in this transitionary regime is obtained as $\hat{V}_f \approx 0.7\hat{V}_t$. This speed decreases as flow goes toward diffusive regime due to the above mentioned interfacial instabilities.

1.2 Motivations and Novelties

The remarkable novelty of our research is that for the first time we investigate the (heat-salinity) double diffusive effects in an inclined setting which is of great fundamental interest. Our experimental methodology, dimensional and dimensionless study and ultrasonic velocimetry have been discussed in chapter 2. Chapter 3 presents benchmarking experiment and our experimental results. Finally, we wrap up with presenting discussion and future works.

2 Experimental methodology

2.1 Experimental Setup

Our experimental setup basically consists of two transparent CPVC, with low thermal conductivity, pipes of 1 meter long and internal diameter of 9.525 millimeters, providing an aspect ratio of 0.0048 ($\delta = \frac{D}{L}$) that are connected with a pneumatic gate valve (VAT Inc.) which operates with pressurized air of 205 kPa. Each pipe has been insulated by a vacuum chamber of -15 psi pressure made of an acrylic duct of square cross section to reduce radial heat loss. Figure 1 represents a schematic of our experimental setup. Both pipes are connected to reservoirs of 40 L volume that are filled with desired solutions. All hosing, connections and valves in this flow loop have been insulated by foam wrap. The convection between the two bulk of fluids involved in our experiments is much higher than axial and circumferential conduction. We have reduced conduction components by using small wall thickness for our pipes ($\approx$ 1.6 mm). We have evaluated and verified the assumption of lowest heat conduction in walls of the pipe by simulating our experimental approach in COMSOL and solving transient heat equations.

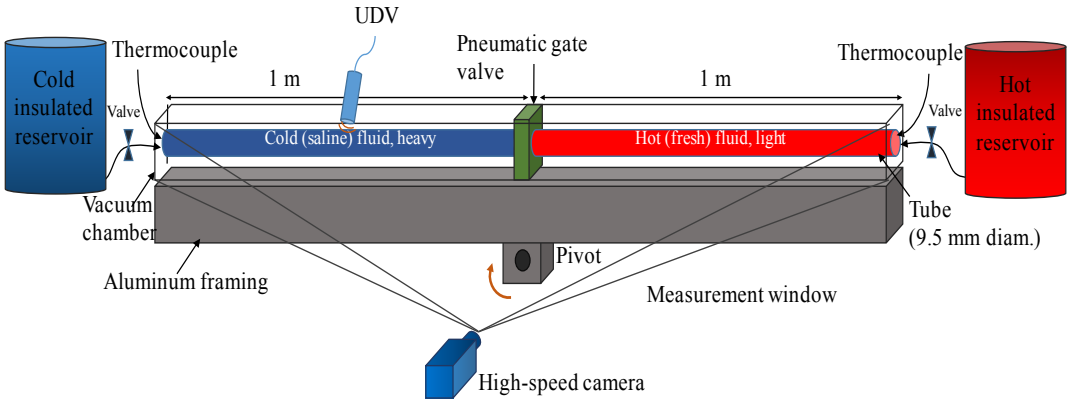

Figure 1. Schematic of experimental setup

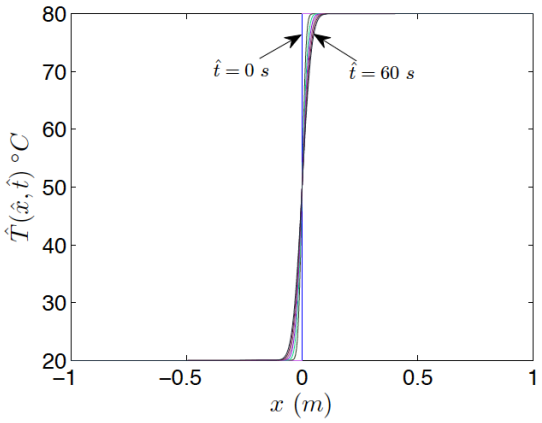

Figure 2. Variation of the temperature, $\hat{T}$, with distance, $\hat{x}$, and time, $\hat{t}$,;based on the solution of (3) using $\hat{T}_{H,0}$ =20℃, $\Delta\hat{T}_0$ =60℃ and $\hat{\alpha}$≈1.4×10^{-7} m^2/s. A negligible distance of maximum 0:08 m on each side of the gate valve seems to have been affected by thermal diffusion prior to the experiments.

For our initial conditions we have considered identical temperature for the whole bulk of cold and hot fluids prior to the start of experiment. The boundary conditions were set as reservoir temperatures. By solving heat transfer equations, we figured that thermal flux through the walls of the pipe is negligible and convection happens between the fluids. Thermal properties of our solutions, such as coefficients of specific heat, $\hat{c}$, thermal conductivity, $\hat{k}$, and thermal expansion, $\hat{\lambda}$, have been obtained from textbooks. Density

measurements have been conducted by DMA 35 density meter from Anton Paar (0.1 kg/m^3 resolution). Rheological characteristics of fluids have been measured over a wide range of temperatures using TA Instruments HR-3 Discovery Hybrid rheometer. Since a Peltier temperature-control surface is provided in this type of rheometers, temperature dependent measurements can be conducted precisely. The viscosity of solutions as a function of temperature is

$$\hat{\mu} = \hat{\mu}_0 e^{-\sigma(\hat{T}-\hat{T}_0)/\hat{T}_0}, \quad (1)$$

where $\hat{\mu}_0$ is reference viscosity of the fluid at room temperature, $\hat{T}_0 \approx 25℃$, and σ is an activation energy parameter [52].

The fluids that has been used in these experiment are water based solutions. Since density unstable configuration is studied the upper section is filled with heavier fluid and lighter fluid is placed in the lower part. Density difference between fluids either comes from temperature gradient or a densifying agent such as NaCl (in double diffusion cases). In order to provide the required temperature differences, fluid tanks are equipped with band heaters. Retaining temperature is very crucial to keep Atwood number, $At = \frac{\hat{\rho}_H - \hat{\rho}_L}{\hat{\rho}_H + \hat{\rho}_L}$, constant. As a result, fluid tanks and all other connections have been insulated by fiber glass and foam wraps respectively. Both fluids consist of polyamide seeding particles (psp) of 50 μm diameter for velocimetry purposes using an Ultrasonic Doppler Velocimeter (UDV). Black ink has been added to displaced fluid (lighter fluid) so that a range of different concentrations can be captured optically. Accumulation of these additives has been measured in a way to achieve concentration field using physical light absorption laws (beer Lambert) and not to affect the fluid properties. Images are captured with high speed camera (Basler Ace acA2040-90um CMOS, 2048^2 pixels) with $2^{12} (= 4096)$ gray scale

levels and a high resolution lens (16 mm F/1.8 C-mount) 8 Hz recording rate. A domain of 97 centimeters of each pipe has been covered. LED stripes light the pipes from 1 side and light diffuser sheet between LED and pipes provide a dispersed lighting. Color map spatio-temporal and finger snapshots are the result of processing these grey scale images via MATLAB. All recordings have been captured for 30 seconds.

Prior to opening the gate valve, we want to make sure that there is sharp temperature gradient at both interfaces and natural convection is not affecting the buoyancy driven exchange flow. In order to evaluate these two criteria, critical Rayleigh number for a small aspect ratio configuration should be calculated and if the corresponding Rayleigh number for our geometry is below this critical number, heat transfer is mainly in the form of conduction and we can neglect natural convection effect. The critical value has been indicated as $Ra_{cr} \approx O(10^{11})$, in the literature [88]. In the worth case of vertical inclination, Rayleigh number, $Ra \approx O(10^{3})$, is much smaller. Our velocity measurements and dynamic studies also clarify this fact. We need to have a sharp temperature difference on both sides of the gate valve before starting the experiment. This can be confirmed by solving heat diffusion equation

$$\frac{\partial \hat{T}}{\partial \hat{t}} = \hat{\alpha} \frac{\partial^2 \hat{T}}{\partial \hat{x}^2}, \tag{2}$$

where, $\hat{T}$ denotes temperature, $\hat{\alpha} = \hat{k}/(\hat{\rho}_0 \hat{c})$ shows thermal diffusivity, $\hat{t}$ and $\hat{x}$ represent time and stream-wise distance respectively, $\hat{k}$ is the fluids' common thermal conductivity, and $\hat{\rho}_0$ indicates the initial mean density of the fluids. The solution of equation (2) is given in the following complementary error function form

$$\hat{T} = \hat{T}_{H,0} + \frac{\Delta \hat{T}_0}{2}\, erfc\,(\frac{\hat{x}}{2\sqrt{\hat{\alpha}\hat{t}}}), \tag{3}$$

where, $\hat{T}_{H,0}$ and $\hat{T}_{L,0}$ are initial temperature of hot and cold fluids respectively. Here, $\Delta\hat{T}_0 = (\hat{T}_{L,0} - \hat{T}_{H,0})$ is the temperature difference of the two fluids at initial condition. The temperature variation over the whole length of the pipes for 60 seconds have been plotted in **Figure 2**. The results have been generated using a thermal diffusivity of approximately $\alpha \approx 1.4\times10^{-7}\ m^2/s$ (representing water). Only a small portion on each side of the gate (3 *cm*) valve have been affected by temperature gradient of fluids, which is in a good agreement with the assumption of sharp temperature gradient. Dual thermocouples were connected to a data logger (ISD-TC, Omega Engineering Inc.) in order to control temperature of bulk fluids in the reservoirs over the entire time of experiment. Because of the finite length of the pipes used in the experiments, a small temperature drop took place in hot fluid over time. As a result, we stopped the experiments when the error in Atwood number reached 7%.

We have made sure that our flow loop works properly by both designing benchmarking experiments and validating our results with that of in the literature. Moreover, same experiments have been repeated and results comparison approves precise measurements presented in chapter 3, in both cases.

2.2 Range of Dimensional and Dimensionless Parameters

A dimensional analysis of the non-isothermal flow suggests that there can be more than 15 dimensionless parameters governing the flow. In order to draw any physical conclusion from the study, we inevitably have to narrow down our scope. In this regard, it is assumed that our pair fluids are liquid, incompressible and Newtonian and have approximately the same coefficients of specific heat, $\hat{c}$, thermal expansion, $\hat{\lambda}$, and conductivity, $\hat{k}$. We further assume that the pair fluids are miscible. Non-isothermal interpenetrative flow of immiscible fluids is governed by completely different dynamics than the miscible limit which is not within our scope. The geometric

dimensionless parameters are namely tube inclination, β, measured from vertical, and aspect ratio, $\delta = \frac{D}{L}$, chosen to be small ($\delta \ll 1$), in order to capture the effects for fully-developed flows. In order to understand the basic thermal effects occurring between the two fluids, a solid pipe with negligible thermal conductivity is considered.

Consequently, the heat transfer within the pipe wall in axial, circumferential and radial (adiabatic) directions would be insignificant. Initially, the cold heavy fluid has temperature $\hat{T}_{H,0}$ and density $\hat{\rho}_{H,0}$ and is denoted by scalar concentration $c = 0$. Similarly, the hot light fluid has temperature $\hat{T}_{L,0}$ and density $\hat{\rho}_{L,0}$ prior to the start of the flow and is denoted by concentration $c = 1$. The dimensionless temperature difference ratio is denoted by $r_T = \frac{\Delta\hat{T}_0}{\hat{T}_{H,0}}$, where $\Delta\hat{T}_0 = \hat{T}_{L,0} - \hat{T}_{H,0}$. The Atwood number, based on the fluids initial densities, is defined as $At_0 = \frac{\Delta\hat{\rho}_0}{2\hat{\rho}_0}$, representing a dimensionless density difference, where $\Delta\hat{\rho}_0 = \hat{\rho}_{H,0} - \hat{\rho}_{L,0}$, and $\hat{\rho}_0 = (\hat{\rho}_{H,0} + \hat{\rho}_{H,0})/2$ are the density difference and the mean density respectively. Note that the density difference between the two fluids might originate from a temperature difference, a densifying agent such as salt or a combination of both. We consider a case where salinity and heat are added to the heavy and light fluids respectively i.e. density-unstable configuration ($At_0 > 0$). Our focus in this study is on small At_0, the significance of which is that a Boussinesq approximation is valid. Briefly, this means that density differences can significantly affect the buoyancy force but not the acceleration of individual fluids.

The effects of thermal expansion of the fluids on driving buoyancy force is retained in the Grashof number defined as $Gr = \hat{g}\hat{\lambda}\Delta\hat{T}_0\hat{D}^3/v^2$. Here, $\hat{D}$ is the tube diameter, $\hat{g}$, the gravitational acceleration and $\hat{v}$, the kinematic viscosity defined using the mean density, $\hat{\rho}_0$, and the viscosity of the heavy fluid, $\hat{\rho}_{H,0}$. Another dimensionless parameter is the Reynolds number defined as, $Re = \hat{V}_t\hat{D}/\hat{v}$, where $\hat{V}_t = (At_0\,\hat{g}\hat{D})^{1/2}$ is a velocity scale obtained from the balance of the buoyant,

$\Delta\hat{\rho}_0\hat{g}\hat{D}$, and inertial, $\hat{\rho}_0\hat{V}^2$, stresses. The viscosity ratio is denoted by $m = \hat{\mu}_{L,0}/\hat{\mu}_{H,0}$. We assume that the viscosity of the fluids weakly depends on temperature i.e. the limit of small Nahme number defined as $Na = \sigma\hat{\mu}_{H,0}\hat{V}_t{}^2/(\hat{k}_{H0}\hat{T}_{H,0})$, where σ is an activation energy parameter representing the sensitivity of the viscosity to temperature variation. The ratio of viscous to thermal diffusivity in our convective flow is captured through the Prandtl number defined as $Pr = \hat{v}/\hat{\alpha}$. Here, $\hat{\alpha} = \hat{k}/\hat{\rho}_0\hat{c}$ is the common thermal diffusivity of the fluids used to measure how rapid the fluids conduct thermal energy as opposed to store it. The degree of molecular diffusive transport compared to advective transport is governed by the Peclet number, $Pe = \frac{\hat{V}_t\hat{D}}{\hat{D}_m}$, where $\hat{D}_m$ is the molecular diffusion. We further concentrate on the limit where molecular diffusion is very small, quite commonly observed in nature and industry where the fluids involved are mostly water based solutions with self-diffusivity of $\hat{D}_m \approx O(10^{-9})\ m^2/s$.

The small molecular diffusion results in high Peclet number regime ($Pe \gg 1$), which inevitably approaches the zero surface tension immiscible limit, provided the interface remains stable [24, 25]. Note that although the Peclet number considered in our study is large, the effects of mass diffusion can be quite significant when there is strong mixing and turbulence occurring in the flow [9, 26]. The ratio of thermal to mass diffusivity is characterized by the Lewis number, Le, expressed as $Le = \frac{\hat{\alpha}}{\hat{D}_m} = \frac{Pe}{Re.Pr}$. Note that due to the choice of fluids and range of temperature differences considered, viscous dissipation effects captured via the Brinkman number, $Br = \hat{\mu}_{H,0}\hat{V}_t{}^2/\hat{k}\Delta\hat{T}_0$, are negligible ($Br \ll 1$). A final note here is that other relevant dimensionless numbers such as Rayleigh number, Ra, Nusselt number, Nu, and Eckert number, Ec, can be constructed as a function of those represented above as $Ra = Gr.Pr$, $Nu = f(Re, Pr)$, and $Ec = Br/Pr$ respectively. In summary, the *independent* input parameters of the problem are β, $\hat{g}$, $\hat{D}$, $\hat{L}$, $\hat{c}$, $\hat{\lambda}$, $\hat{k}$, $\hat{T}_{H,0}$, $\hat{T}_{L,0}$, $\hat{\rho}_{H,0}$, $\hat{\rho}_{L,0}$, $\hat{\mu}_{H,0}$, $\hat{\mu}_{L,0}$, $\hat{D}_m$ and σ listed in **Table 1**. In the *dimensionless* space,

these parameters reduce to β, δ, r_T, At_0 , Gr, Re, m, Na, Pr, Pe and Br.

As will later be explained, our methodology is designed to understand the effect of various parameters of the problem in a step-by-step manner over isolated ranges of $\delta \ll 1$, $Pe \gg 1$, $Br \ll 1$, and $Na \ll 1$. The dimensionless numbers governing the flow in question are listed in **Table 2**, along with the range considered.

Table 1. List of dimensional independent input parameters of the problem.

Parameter	Range
β	$0 - 90°$
$\hat{g}$	$9.8\ m/s^2$
$\widehat{D}$	$9.53\ mm$
$\hat{L}$	$2\ m$
$\hat{c}$	$4.18\ kJ/(kg.K)$
$\hat{\lambda}$	$0.0002 - 0.0005\ 1/K$
$\hat{\kappa}$	$0.28, 0.58\ W/(m.K)$
$\hat{T}_{H,0}$	22℃
$\hat{T}_{L,0}$	$40 - 75$℃
$\hat{\rho}_{H,0}$	$998\ kg/m^3$
$\hat{\rho}_{L,0}$	$960\ kg/m^3$
$\hat{\mu}_{H,0}$	$0.001\ Pa.s$
$\hat{\mu}_{L,0}$	$0.0005\ Pa.s$
$\widehat{D}_m$	$10^{-9} - 10^{-11}\ m^2/s$
σ	2

Table 2. List of dimensionless independent input parameters of the problem

Parameter	Range
β	$0 - 90°$
$\delta = \frac{\widehat{D}}{\widehat{L}}$	≈ 0.0048
$r_T = \frac{\Delta\widehat{T}_0}{\widehat{T}_{H,0}}$	$r_T \approx O(1)$
$At_0 = \frac{\Delta\hat{\rho}_0}{2\hat{\rho}_0}$	$0.0035, 0.01$
$Gr = \hat{g}\hat{\lambda}\Delta\widehat{T}_0\widehat{D}^3/v^2$	$0 \leq Gr \leq O(10^6)$
$Re = \widehat{V}_t\widehat{D}/\hat{v}$	$0 \leq Re \leq O(10^3)$
$m = \hat{\mu}_{L,0}/\hat{\mu}_{H,0}$	$0.5, 1, 2$
$Na = \sigma\hat{\mu}_{H,0}\widehat{V}_t{}^2/(\hat{k}_{H0}\widehat{T}_{H,0})$	$Na < 1$
$Pr = \hat{v}/\hat{\alpha}$	$Pr \approx O(1)$
$Pe = \frac{\widehat{V}_t\widehat{D}}{\widehat{D}_m}$	$Pe \gg 1$
$Br = \hat{\mu}_{H,0}\widehat{V}_t{}^2/\hat{k}\Delta\widehat{T}_0$	$Br \ll 1$

2.3 Ultrasonic Doppler Velocimetry (UDV)

In order to better understand front dynamics, we have conducted an Ultrasonic Doppler Velocimetry (UDV). The UDV probe is installed in the middle section of the lower pipe. Polyamid Seeding Particles (PSP) have been added to both solutions to an extent that

doesn't change fluids' properties. Ultrasonic wave excites these particles and the corresponding velocity will be recorded The axial resolution of UDV within the depth of our fluids is about 0.128 *mm* and the lateral resolution is equal to the transducer diameter (8 *mm*), slightly varying with depth. A 4-*MHz* transducer has been used in our signal processing measurements. The probe is mounted outside the pipe, so it does not interfere with flow. Recorded velocities are in a depth wise direction. More information has been presented in chapter 3.

3 Results

In this section our experimental results have been presented. Main characteristics of a typical double diffusive buoyancy driven exchange flow will be discussed following with comparing our approach with existing results in literature by conducting benchmarking experiments [13]. Front dynamics and measuring the propagating velocity of both fingers is crucial in understanding the displacement of fluids and the exchange phenomenon. Regime classification based on different pipe inclination angles is also discussed.

The asymmetry of the heavy and light fingers was recorded as the most significant feature in this phenomena. Due to the vacuum chamber that surrounds the pipes, the radial heat loss from the pipe to the ambient is negligible. The accuracy of this assumption has been confirmed by COMSOL simulation. **Figure 3(a)** represents the snapshots of a typical isothermal exchange flow that was done for the salt-water displacing pure water at $\beta = 60°$, and **Fig. 3(b)** shows the snapshots for a Double Diffusion case with both temperature gradient and salt as densifying agent instead of salinity, which can cause formation of some instabilities at the interfaces.

Considering the blue tip (concentration of 0) in isothermal case in comparison with a green fingertip (concentration of 0.5) for double diffusion experiments, it is evident that more mixing happens in latter one. Conservation of mass law can be explained by different thickness of fingers, where the thinner finger propagates to a longer extend while the thicker one grows less in longitudinal direction.

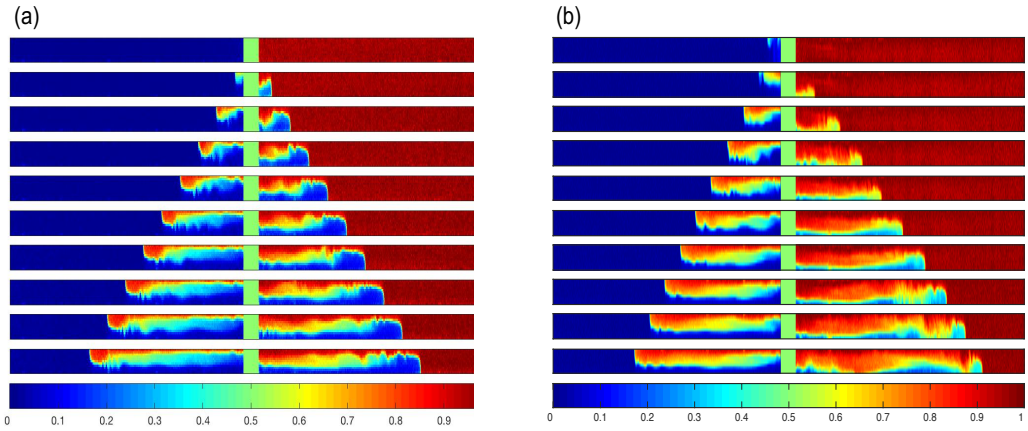

Figure 3. Snapshots of the exchange flow carried for $\beta = 60°$: (a) Isothermal study, $\hat{\rho}_{H,0} = 1017.7\ Kg/m^3$, $\hat{\rho}_{L,0} = 997.5\ Kg/m^3$). (b) Double diffusion study, $\hat{T}_{H,0} = 25$ ℃, $\hat{T}_{L,0} = 52.2$ ℃, $\hat{\rho}_{H,0} = 1007.1 Kg/m^3$, $\hat{\rho}_{L,0} = 987\ Kg/m^3$, $\hat{\mu}_{H,0} = 8.8\times10^{-4}\ Pa.s$, $\hat{\mu}_{L,0} = 5.3\times10^{-4}\ Pa.s$.

Snapshots of isothermal and double diffusion depicts the fraction of heavy fluid with inclination angle from horizontal to vertical that inspired by the transverse gravity component. Three different regimes were observed for isothermal (**Fig. 4(a)**) and double diffusion study (**Fig. 4(b)**). For the horizontal pipe, the buoyancy and viscous forces are balanced that results in a Poiseuille-like, counter-flow of two fluids with no mixing, and the buoyancy term is dissipated by viscosity. The balance between buoyancy and viscous terms gives the viscous velocity: $\hat{V}_v = {(At\hat{g}\hat{D})\text{^}2}/{v}$ Close to the vertical, the balance between buoyancy and inertia leads to: $\hat{V}_t = \sqrt{At\hat{g}\hat{D}}$ As the tilt angle increases from horizontal to vertical, the mixing becomes stronger due to Kelvin-Helmoltz instabilities for miscible fluids. When the segregation is affected by transverse mixing, the flow pattern alternates from viscous to intermittent phase. During this transition, the front velocity reaches a plateau value equal to $0.7\hat{V}_t$.

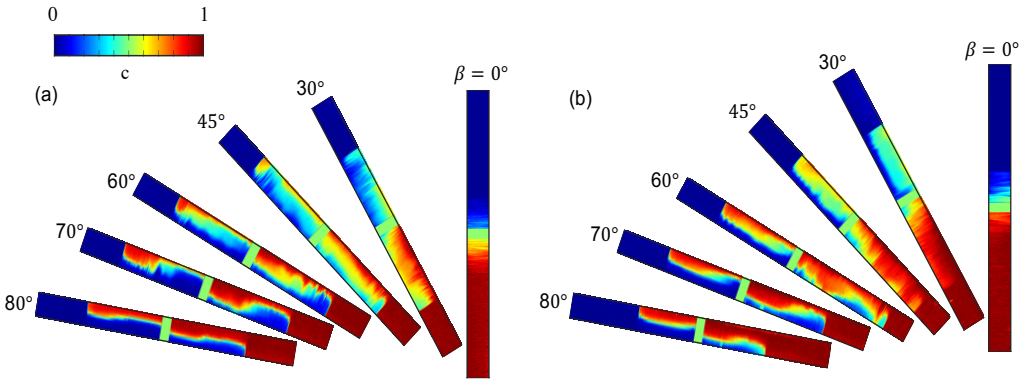

Figure 4. (a) Change in isothermal exchange flow with β, (b) Double diffusion exchange flow. The color bar at the top left of the figure shows the corresponding concentration value, c, with 0 referring to the pure displacing fluid and 1 to the pure displaced fluid.

Due to the back-lighting and imaging technique used in our study, the concentration values, C, captured with the camera have already been averaged in the transverse ($\hat{z}$) direction. Therefore, $C = C(\hat{x}, \hat{y}, \hat{t})$ only. It is useful to define the depth-averaged concentration, $\bar{C}$, as

$$\overline{C}\,(\hat{x}, \hat{t}) = \frac{\int_0^{\hat{D}} C(\hat{x}, \hat{y}, \hat{t})\; d\hat{y}}{\hat{D}}. \tag{4}$$

The depth-averaged concentration $\overline{C}\,(\hat{x}, \hat{t})$ does not give any information whether or not the flow is symmetric in the transverse direction, however, it provides us with some very useful information about how much heavy and/or light fluids exist in a given stream-wise location, $\hat{x}$, at time $\hat{t}$ ($\overline{C} = 0.1$) correspond to pure heavy and light fluid layers respectively). When the flows fully mix transversely, it is logical to assume a rather stationary mixing core and use $(\hat{x})/\sqrt{\hat{t}}$ as a similarity scaling [16]. In this case the dynamics of the flow is governed by a linear diffusion equation

$$\frac{\partial \overline{C}}{\partial \hat{t}} = \hat{D}_M \frac{\partial^2 \overline{C}}{\partial \hat{x}^2}. \tag{5}$$

Here, $\widehat{D}_M$ is a macroscopic diffusion coefficient which could be up to 10^5 times bigger than the molecular diffusivity, $\widehat{D}_m$ [24]. The solution of equation (5) can then be found in the following form

$$\widehat{D}_M = 5{\times}10^3(\hat{V}_t\widehat{D})(1+3.6\,tan\beta)^2(\frac{\hat{V}_t}{\hat{V}_v})^{3/2}, \tag{6}$$

where $V_v = \frac{At\,\widehat{g}\,\widehat{D}^2}{v}$ is a velocity scale obtained from the balance between buoyant and viscous forces. Note that the range of applicability of 7 in [16] is for $Re \leq 1000$, which covers the range of our exchange flow experiments. In order to check the consistency of our macroscopic diffusion coefficient measurements, the data are compared with [14] in **Fig. 5**, for those of our isothermal experiments that were fully mixed. The agreement is good, with a similar deviation as for the data in [16].

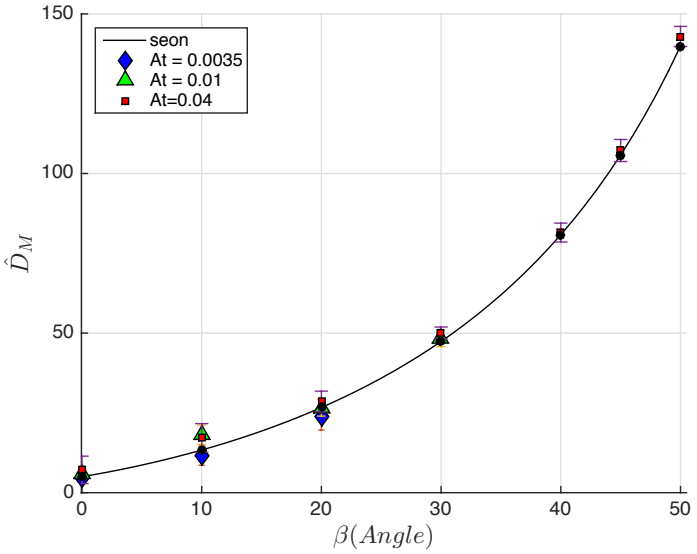

Figure 5. Variation of the dimensionless macroscopic diffusion coefficient versus tilt angle. The crosses are based on our measurements for $At = 0.04$, triangles for $At = 0.01$ and squares for $At = 0.0035$, and circles are added from Seon et al. [14] experiments.

In the benchmarking step, an error function was applied to fit the best curve on the concentration profile as $C = 0.5\,\mathrm{erf}\left(\frac{\hat{x}}{\sqrt{\widehat{D}_M\hat{t}}}\right)$. The fitted curve gives the macroscopic

diffusion coefficient $\widehat{D}_M$. The same process was studied by Seon et al., and the following equation shows the measured $\widehat{D}_M = 5\times10^3(\hat{V}_t\widehat{D})(1+3.6\,tan\beta)^2(\frac{\hat{V}_t}{\hat{V}_v})^{3/2}$. **Figure 5** exhibits that our macroscopic diffusion coefficients are in an excellent agreement with that of Seon's results [14].

Figure 6 displays the spatial-temporal diagrams for the same snapshots as shown in **Fig. 4(b)** which represent the depth-averaged concentration along the pipe. As can be seen in **Fig. 6 (d, e, f)** the fluids are separated for viscous regimes with a sharp interface, while the boundary of fluids becomes more unstable and difficult to recognize for diffusive flows as shown in **Fig. 6 (a, b).** Again the asymmetry of flows is evident on each side of spatial-temporal graph.

Figure 7(a) represents how we use concentration field to measure velocity. As the heavy fluid moves in x direction and enters the other section of pipe which is initially filled with light fluid a threshold of 0.1 has been defined so as it occupies 0.1 of the pipe in y direction it will be captured as the tip of the finger and the velocity can be measured over time as the finger propagates along pipe, and the same procedure has been followed for the other half of the pipe. The dashed lines indicate the concentration threshold on each side of the pipe. **Figure 7(b)** shows the evolution of heavy and light finger velocities. Since by opening the gate valve flows start from rest (zero velocity) a huge velocity will be detected at initial time and as the flows spread forward, the velocities become more stable. $\hat{V}_{f,H}$ stands above $\hat{V}_{f,L}$ graph which suggests the asymmetry in our experiments.

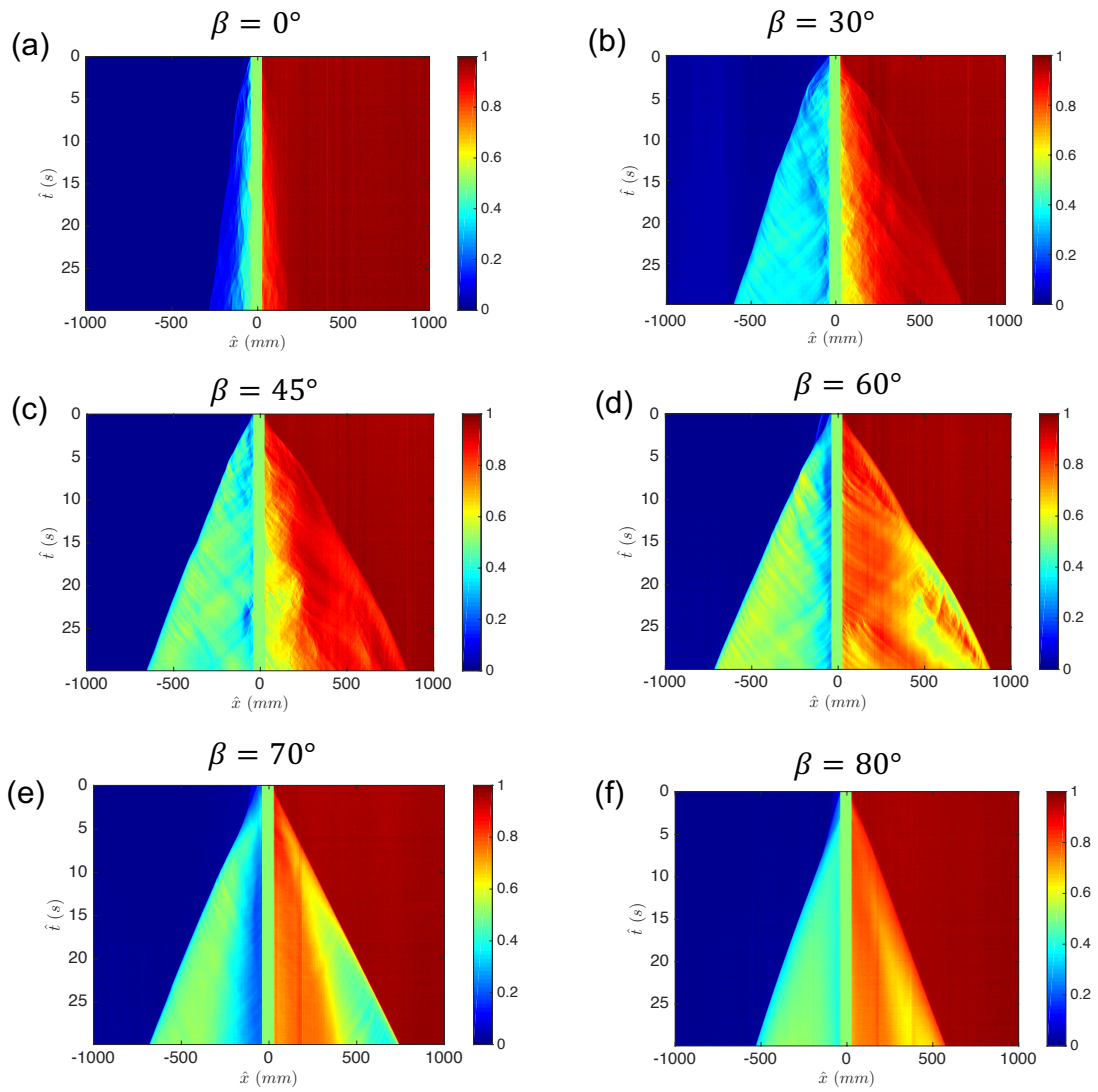

Figure 6. Spatiotemporal diagrams of depth-averaged concentration field, $\bar{C}_{\hat{y}}(\hat{x},\hat{t})$, for the same experiments as shown in Spatiotemporal (a) $\beta = 0°$, (b) $\beta = 30°$, (c) $\beta = 45°$, (d) $\beta = 60°$, (e) $\beta = 70°$, (f) $\beta = 80°$.

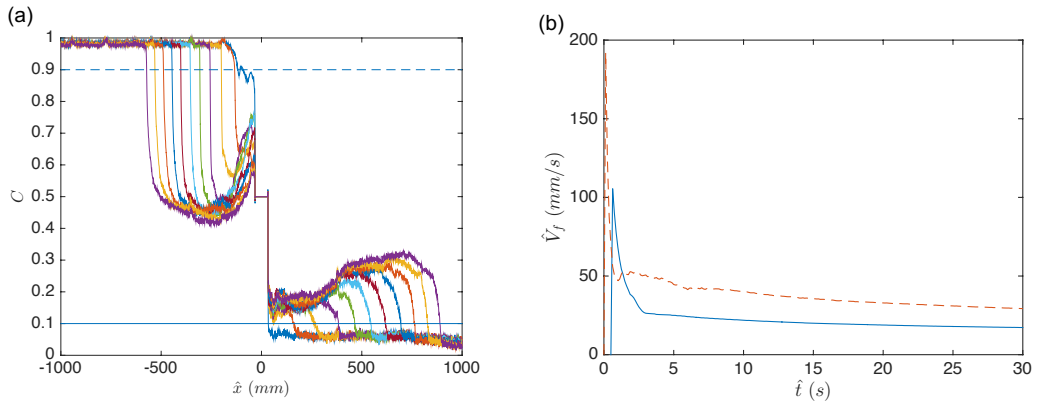

Figure 7. (a) Evolution of the depth-averaged concentration, $\bar{C}_{\hat{y}}(\hat{x},\hat{t})$, with time, and location. The blue solid and dashed lines show $\bar{C}_{\hat{y}}$=0.1 and $\bar{C}_{\hat{y}}$=0.9 (threshold for measuring the displacing and trailing front velocities) respectively. (b) Evolution of displacing and trailing front velocity, with time.

In **Fig. 8** evolution of front velocity for both heavy and light fluids based on tilt angle, β, has been indicated. It is clear that velocity of heavy fluid is higher than that of light fluid in all angles, and higher density difference, Atwood number, results in higher velocities for the finger to propagate. As we go from low tilt angles to high inclination angles, the flow regime has a transition from viscous to intermittent and diffusive respectively, and the velocity increases until it reaches a peak in the intermittent regime and then drops.

To further investigate the asymmetrical finger growth, complementary experiments have been designed adding glycerol to both sides to have a solution of 20 and 50 percent by weight of water glycerol. This solution has a higher viscosity than water but lower thermal diffusivity. Again an asymmetrical fingering occurs at different tilting angles. Same experiment was done by adding xanthan gum to water. Xanthan gum does not change thermal properties of water while it increases the viscosity of the solution. Unsymmetrical fingers propagate in this case as well.

In order to further investigate the effect of viscosity and thermal gradient on asymmetrical configuration, we decided to add xanthan gum to the heavy fluid and use

sodium chloride as densifying agent to eliminate thermal effects while providing a viscosity ratio for our solutions. Xanthan gum is a great choice since it is soluble in water and does not affect thermal properties of it nor changes its density, but it can increase the viscosity of water. Interestingly a symmetrical fingering was observed in this experiment, **Fig. 9**, suggesting that the asymmetry should be a result of temperature dependent parameters of the phenomena.

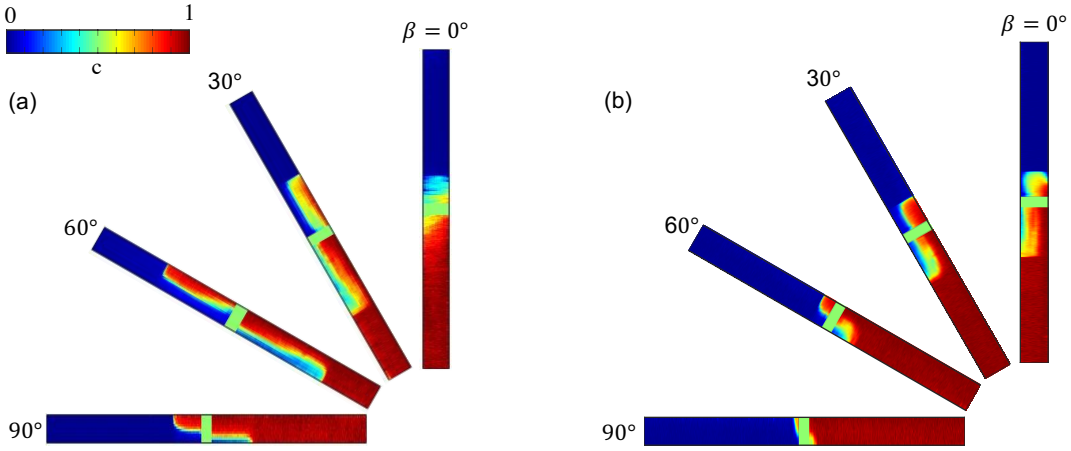

F**igure 8**. Snapshots of experiments for non-isothermal exchange flow for (a) Glycerol-water solution. (b) Xanthan-water solution.

Figure 10 represents an experiment in which the heavy fluid is the hot salt-water and the light fluid is pure cold water. Here it has been expected to observe asymmetrical fingering where the cold light finger penetrates longer distance. Same as the behavior of cold heavy finger in **Fig. 3(b)**. Since the wall of the pipe in hot side conserves its temperature, while the cold fluid enters the hot media, the hot area adjacent to the wall provides a lower viscous region of fluid which serves as a lubrication layer and accelerates the movement of the cold finger. This is why in both cases, where the cold finger was heavy or light, a longer finger for cold fluid was observed.

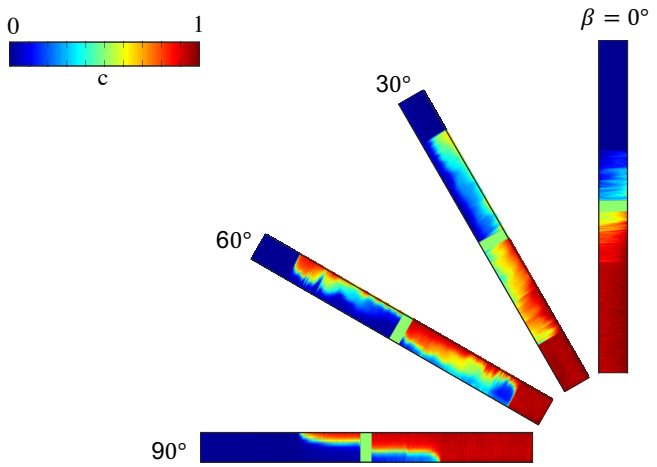

Figure 9. Snapshots of isothermal exchange flow with Xanthan added to heavy (salt-water) fluid with $\hat{\rho}_{H,0} = 1017.7\ Kg/m^3$, $\hat{\rho}_{L,0} = 997.5\ Kg/m^3$, $\hat{\mu}_{H,0} = 0.002\ Pa.s$, $\hat{\mu}_{L,0} = 8{\times}10^{-4}\ Pa.s$, at time $\hat{t} = 30.0\ s$. The color bar at the top left of the figure shows the corresponding concentration value.

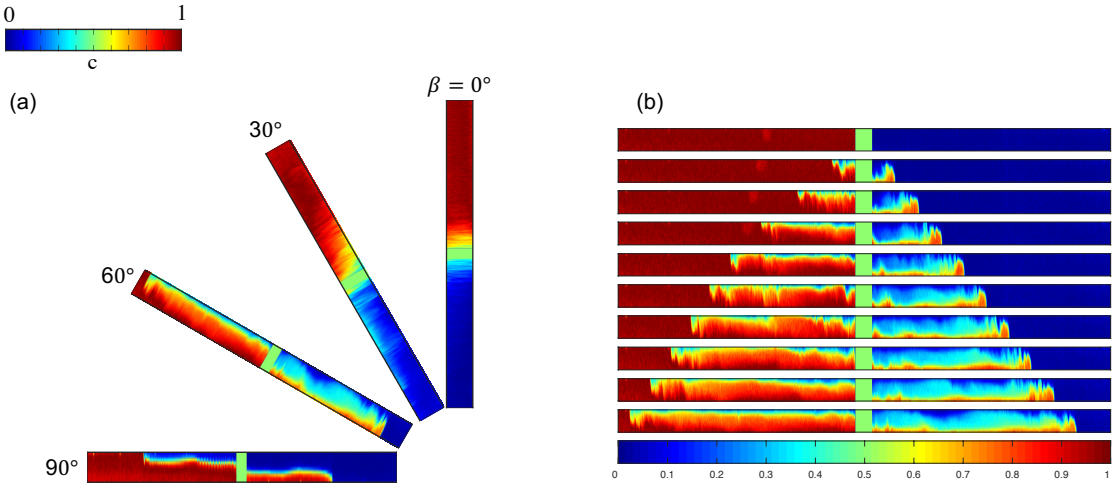

Figure 10. Snapshots of experiments for double diffusion exchange flow with salt added to hot water, (a) Change in flow by inclination angle, β, at time $\hat{t} = 30.0\ s$. (b) Experiment carried for $\beta = 60°$, at times $\hat{t} = [0,\ 3.33,\ 6.66,\ \ldots, 26.67,\ 30.0]\ s$.

In **Fig. 11**, finger velocity of heavy and light fluids has been measured using the same approach as mentioned in **Fig. 7** Velocity Reading (a) and they indicate a higher velocity for the heavy finger which propagates in hot media and supports the idea of lubrication of

low viscous solution resulting in asymmetrical growth.

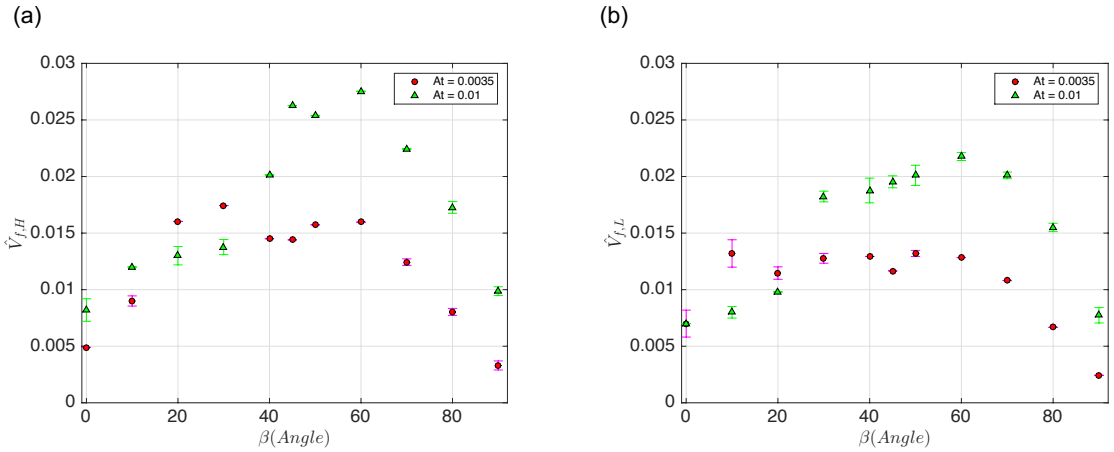

Figure 11. Change in (a) heavy front velocity, $\hat{V}_{f,H}$, and (b) light front velocity, $\hat{V}_{f,L}$, with tilt angle, β. Different markers represent $At = 0.0035$ (●), 0.01 (△). The dashed lines are guide to the eye.

Figure 12 indicates evolution of front dynamics in different flow regimes. As we go from lower inclination angle to higher angles, 30 to 60 degree, thus transition from intermittent to viscous regime, a flattened front has been observed in UDV measurements. In this graph asymmetry has been quantified as a dimensionless parameter, e, which is defined as $\frac{\hat{V}_{f,H}-\hat{V}_{f,L}}{\hat{V}_t}$ and has been plotted versus inclination angle, β, which gives us an insight about how this asymmetry varies in different tilting angles and Atwood numbers.

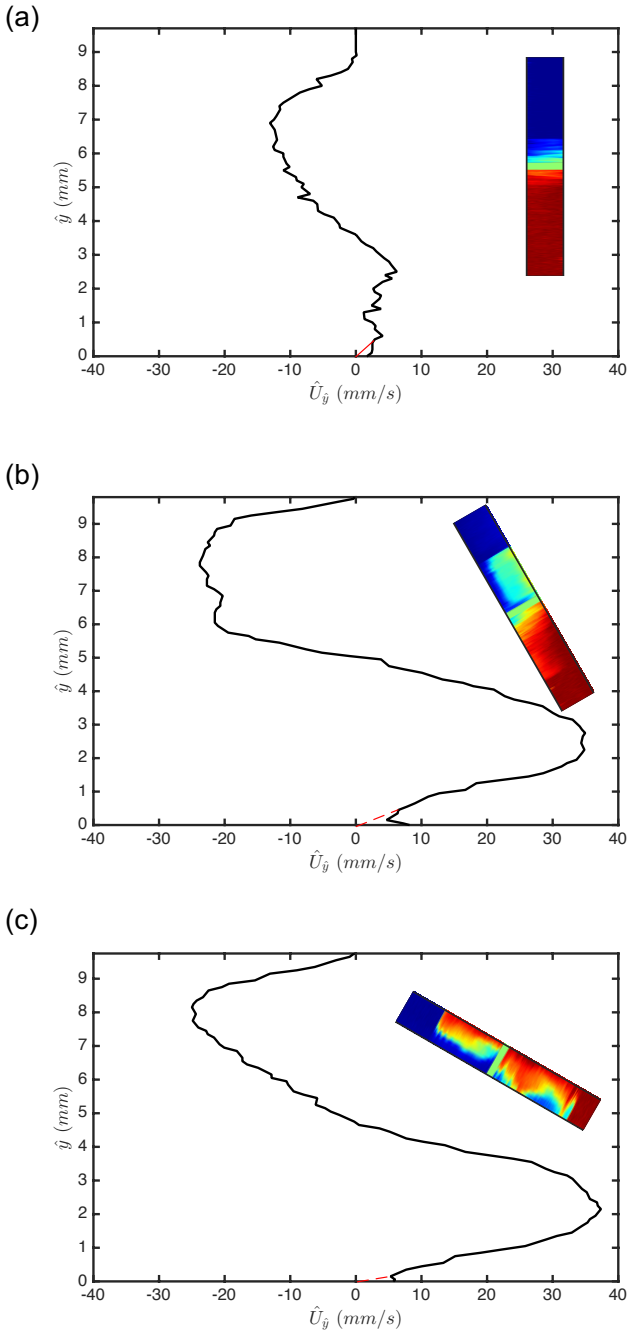

Figure 12. Change in front dynamic with inclination angle for double diffusion study, $(a)\ \beta = 30°, \hat{t} \in [21.0, 25.0]s.\ (b)\ \beta = 60°, \hat{t} \in [23.0, 27.0]$

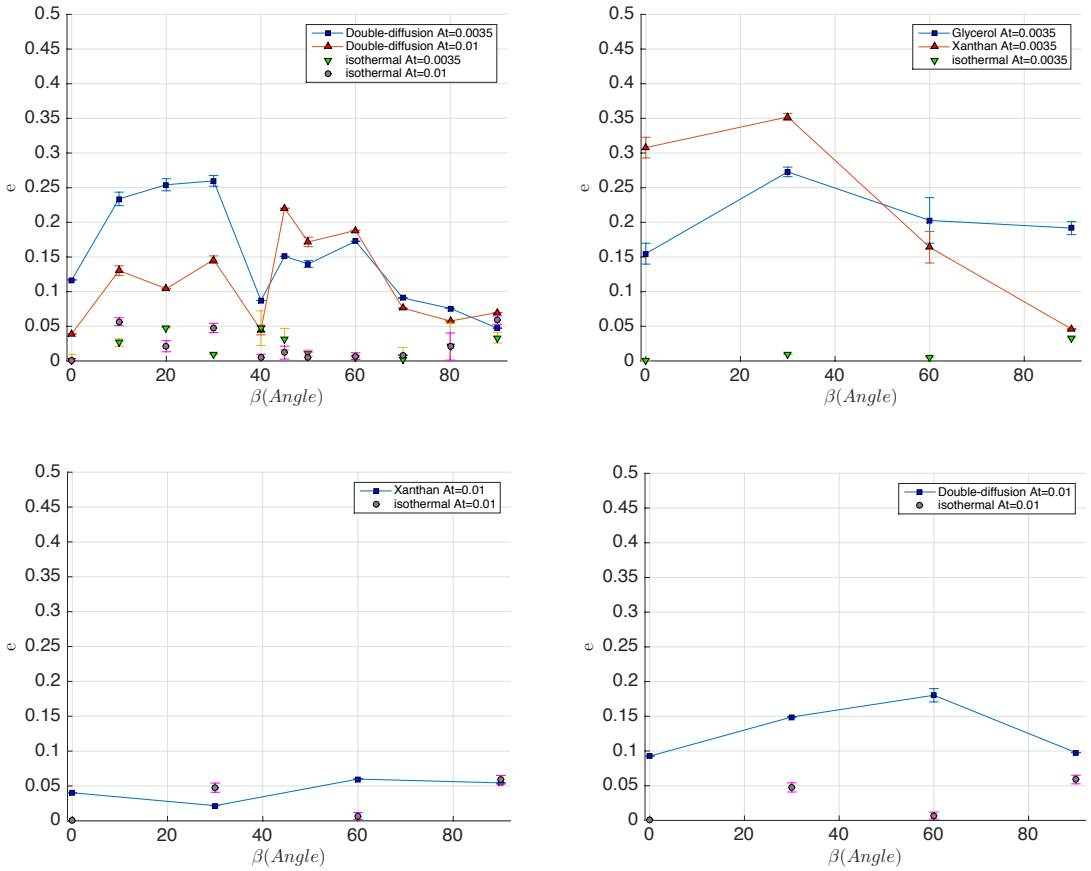

Figure 13. Change in asymmetry with inclination angle for (a) Double-diffusion (b) Glycerol and Xanthan solutions study (c) Xanthan added to one side study (d) Double diffusion case where both heat and salt have been added to one side study, all versus isothermal experiment.

4 Discussion and future works

Buoyancy-driven exchange flow of two Newtonian fluids in an inclined pipe has been investigated experimentally when there is a temperature difference between the fluids i.e. non-isothermal. The cold heavy fluid is released into the hot light one due to the buoyancy in an adiabatic pipe with small aspect ratio. Due to the choice of low Atwood numbers, Boussinesq approximation holds. Our experiments cover a broad range of the governing dimensional and dimensionless parameter space, not covered before in any experimental study. Detailed benchmarking tests were first made upon the established exchange flow studies of [13-16] in the isothermal limit revealing excellent qualitative and quantitative agreement in flow classification, frontal velocity and macroscopic diffusion coefficient. *Viscous* regimes are found at near-horizontal inclination angles. The degree of flow instability and mixing enhances as the pipe is progressively inclined towards vertical revealing *intermittent* and *fully diffusive* regimes. Reminiscent to the well-known Boycott effect [54], the maximum interpenetration rate of heavy and light fluids in both isothermal and non-isothermal cases is found to occur at an intermediate inclination angle.

A novel asymmetric behavior in the flow is observed in non-isothermal flows never seen before in the isothermal limit. The heavy cold finger interestingly advances faster than the light hot one for both water and water-glycerin solutions. The phenomenon was first thought to be related to the difference in bulk viscosity of heavy and light fluids due to temperature difference. Additional experiments were then run using more-viscous heavy xanthan-water interpenetrating a less-viscous light water solution in the isothermal limit revealing symmetric flows. This, in turn, suggests that bulk viscosity contrast between the two fluids may not cause the flow asymmetry. The asymmetric behavior is then

hypothetically associated with the wall contact and the formation of a warm less-viscous *film* of the fluid *lubricating* the cold more-viscous finger along the pipe. On the other side of the pipe, a cool more-viscous film forms *decelerating* the hot less-viscous finger. In order to clarify the root of this phenomenon, further supplementary experiments were precisely-designed in which the heat was added to the heavy fluid (densified by salt). The asymmetry was interestingly observed to occur on the opposite side of the tube i.e. cold finger again traveling faster than the hot one, further solidifying the lubricating film hypothesis. Double diffusive effects associated with the diffusion of mass (salinity) and heat are further investigated. In this case and for the same range of density differences, the level of flow asymmetry is found to decrease. The asymmetric behavior of the flow is finally quantified over the full range of non-isothermal experiments carried.

As future work, we are planning to implement real-time measurements of the temperature field (thermography) in our experiments utilizing the Infrared (IR) approach. An IR camera with spectral range of 1.5-5 μm and spatial resolution of 30 μm is in order to be used. As the polycarbonate and acrylic are not transparent in the IR spectrum, we need to choose another type of material for the main tube and vacuum box. In addition to transmission in the visible and IR spectrums, the tube/box material should possess low thermal conductivity to suppress the circumferential and axial conduction along the tube wall. A polymer called Ethylene tetrafluoroethylene (ETFE) may be a good future candidate to be used as pipe and vacuum box material. This polymer has transmission of ~90% in the spectral range of 0.2-2.5 μm and relatively low thermal conductivity of 0.238 W/(m.K). Therefore, we can hopefully visualize the concentration and thermal fields simultaneously in the exchange flow in question. The intergraded flow visualization and

thermography can reveal how closely the temperature and concentration (salinity) fronts follow one another during the evolution of the flow eventually enabling us understand the fundamental double-diffusive effects underlying the flow. It can also give us insight about the nature of the lubricating layers forming underneath the cold finger due to wall contact. The results presented along with future research directions laid out, can potentially provide significant insight into such the fundamental problem of convective flows in inclined settings. Applications are widely found in the context of oceanographic and geophysical flows (thermohaline circulation on continental slopes/shelves, asthenosphere convection underneath sub-ducting lithosphere etc.) as well as atmospheric flows over hills and mountains which can help municipalities design cities and urban areas for improved micro-climate and air quality management.

References

[1] T. Benjamin, "Gravity Currents and Related Phenomena," *J. Fluid Mech*., vol. 31, pp. 209–248, 1968.

[2] D. Hoult, "Oil spreading in the sea," *Annu. Rev. Fluid Mech*., vol. 4, pp. 341–368, 1972.

[3] V. Birman, B. Battandier, E. Meiburg, and P. Linden, "Lock-exchange flows in sloping channels," *J. Fluid Mech*., vol. 577, pp. 53–77, 2007.

[4] F. Senorans, A. Ruiz-Rodrıguez, E. Ibanez, J. Tabera, and G. Reglero, "Optimization of countercurrent supercritical fluid extraction conditions for spirits fractionation," *J. Supercrit*. *Fluids*, vol. 21, no. 1, pp. 41–49, 2001.

[5] M. Raventos, S. Duarte, and R. Alarcon, "Application and possibilities of supercritical co_2 extraction in food processing industry: an overview," *Food Sci. Technol. Int*., vol. 8, no. 5, pp. 269–284, 2002.

[6] M. Baird, K. Aravamudan, N. Rao, J. Chadam, and A. Peirce, "Unsteady axial mixing by natural convection in vertical column," *AIChE J*., vol. 38, p. 1825, 1992.

[7] O. Levenspiel, "Chemical engineering reaction," *Wiley-Eastern Limited, New York*, 1972.

[8] E. Nelson and D. Guillot, *Well Cementing, 2nd Edition*. Schlumberger Educational Services, 2006.

[9] Y. Ito and R. Bowman, "Angle rotor countercurrent chromatography," *Anal. Biochem*., vol. 65, no. 1, pp. 310–320, 1975.

[10] Y. Ito and R. Bhatnagar, “Improved scheme for preparative countercurrent chromatography (ccc) with a rotating coil assembly,” *J. Liq. Chromatogr*., vol. 7, no. 2, pp. 257–273, 1984.

[11] Y. Ito and W. Conway, “High-speed countercurrent chromatography,” 1986.

[12] M. Debacq, J. Hulin, D. Salin, B. Perrin, and E. Hinch, “Buoyant mixing of miscible fluids of varying viscosities in vertical tube,” *Phys. Fluids*, vol. 15, pp. 3846–3855, 2003.

[13] T. Seon, J.-P. Hulin, D. Salin, B. Perrin, and E. Hinch, “Buoyant mixing of miscible fluids in tilted tubes,” *Phys. Fluids*, vol. 16, pp. 103–106, 2004.

[14] T. Seon, J.-P. Hulin, D. Salin, B. Perrin, and E. Hinch, “Buoyancy driven miscible front dynamics in tilted tubes,” *Phys. Fluids*, vol. 17, pp. 031702(1)–(4), 2005.

[15] T. Seon, J.-P. Hulin, D. Salin, B. Perrin, and E. Hinch, “Laser-induced fluorescence measurements of buoyancy driven mixing in tilted tubes,” *Phys. Fluids*, vol. 18, pp. 041701(1)–(4), 2006.

[16] T. Seon, J. Znaien, D. Salin, J.-P. Hulin, E. Hinch, and B. Perrin, “Front dynamics and macroscopic diffusion in buoyant mixing in a tilted tube,” *Phys. Fluids*, vol. 19, pp. 125105(1)–(7), 2007.

[17] J. Znaien, Y. Hallez, F. Moisy, J. Magnaudet, J. Hulin, D. Salin, and E. Hinch, “Experimental and numerical investigations of flow structure and momentum transport in a turbulent buoyancy-driven flow inside a tilted tube,” *Phys. Fluids*, vol. 21, no. 11, pp. 115102(1)–(10), 2009. 26

[18] J. Znaien, F. Moisy, and J.-P. Hulin, “Flow structure and momentum transport for buoyancy driven mixing flows in long tubes at different tilt angles,” Phys. Fluids, vol. 23, pp. 035105(1) – (14), 2011.

[19] Y. Hallez and J. Magnaudet, “Effects of channel geometry on buoyancy-driven mixing,” *Phys. Fluids*, vol. 20, pp. 053306(1) – (9), 2008.

[20] Y. Hallez and J. Magnaudet, “A numerical investigation of horizontal viscous gravity currents,” *J. Fluid. Mech*., vol. 630, pp. 71–91, 2009.

[21] Y. Hallez and J. Magnaudet, “Turbulence-induced secondary motion in a buoyancy-driven flow in a circular pipe,” *Phys. Fluids*, vol. 21, pp. 081704(1) – (4), 2009.

[22] Z. Borden, E. Meiburg, and G. Constantinescu, “Internal bores: an improved model via a detailed analysis of the energy budget*,” J. Fluid Mech*., vol. 703, pp. 279–314, 2012.

[23] Z. Borden and E. Meiburg, “Circulation-based models for Boussinesq internal bores,” *J. Fluid Mech*., vol. 726, p. R1, 2013.

[24] S. Thorpe, “A method of producing a shear flow in a stratified fluid,” *J. Fluid Mech*., vol. 32, pp. 693– 704, 1968. 27

[25] S. Thorpe, “Experiments on instability and turbulence in a stratified shear flow,” *J. Fluid Mech*., vol. 61, pp. 731–751, 1973.

[26] S. Dalziel, P. Linden, and D. Youngs, “Self-similarity and internal structure of turbulence induced by Rayleigh-Taylor instability,” *J. Fluid Mech*., vol. 399, pp. 1–48, 1999.

[27] Y. Couder, N. Gerard, and M. Rabaud, “Narrow fingers in the Saffman-Taylor instability,” *Phys. Rev. A*, vol. 34, no. 6, pp. 5175–5180, 1986.

[28] P. Tabeling, G. Zocchi, and A. Libchaber, “An experimental study of the Saffman-Taylor instability,” *J. Fluid Mech*., vol. 177, pp. 67–82, 1987.

[29] O. Singh and J. Srinivasan, “Effect of Rayleigh numbers on the evolution of double-diffusive salt fingers,” *Phys. Fluids*, vol. 26, no. 6, pp. 062104(1) – (18), 2014.

[30] H. Huppert and R. Sparks, “Double-diffusive convection due to crystallization in magmas,” *Ann. Rev. Earth Planet. Sci*., vol. 12, pp. 11–37, 1984.

[31] O. Singh, D. Ranjan, J. Srinivasan, and K. Sreenivas, “A study of basalt fingers using experiments and numerical simulations in double-diffusive systems,” *J. Geogr. Geol*., vol. 3, no. 1, pp. 42–50, 2011.

[32] J. Leconte and G. Chabrier, “A new vision of giant planet interiors: Impact of double diffusive convection,” *Astron. Astrophys*., vol. 540, pp. A20(1) – (13), 2012.

[33] M. Mishra, A. De Wit, and K. Sahu, “Double diffusive effects on pressure-driven miscible displacement flows in a channel,” *J. Fluid Mech*., vol. 1, pp. 1–19, 2012.

[34] J. Azaiez and M. Sajjadi, “Stability of double-diffusive double-convective miscible displacements in porous media,” *Phys. Rev. E*, vol. 85, no. 2, pp. 026306(1) – (10), 2012.

[35] M. Sajjadi and J. Azaiez, “Dynamics of fluid flow and heat transfer in homogeneous porous media,” *Can. J. Chem. Eng*., vol. 91, no. 4, pp. 687–697, 2013.

[36] J. Turner and H. Stommel, “A new case of convection in the presence of combined vertical salinity and temperature gradients,” *Proc. Natl. Acad. Sci*., vol. 52, no. 1, pp. 49–53, 1964.

[37] R. Schmitt, “Double diffusion in oceanography,” *Ann. Rev. Fluid Mech*., vol. 26, no. 1, pp. 255–285, 1994.

[38] J. Lee, M. Hyun, and K. Kim, “Natural convection in confined fluids with combined horizontal temperature and concentration gradients,” *Int. J. Heat Mass Tran*., vol. 31, no. 10, pp. 1969–1977, 1988.

[39] H. Han and T. Kuehn, “Double diffusive natural convection in a vertical rectangular enclosure I. experimental study,” Int. J. Heat Mass Tran., vol. 34, no. 2, pp. 449–459, 1991. 29

[40] H. Han and T. Kuehn, “Double diffusive natural convection in a vertical rectangular enclosure II. numerical study,” *Int. J. Heat Mass Tran*., vol. 34, no. 2, pp. 461–471, 1991.

[41] C. Beghein, F. Haghighat, and F. Allard, “Numerical study of double-diffusive natural convection in a square cavity,” *Int. J. Heat Mass Tran*., vol. 35, no. 4, pp. 833–846, 1992.

[42] M. Corcione, S. Grignaffini, and A. Quintino, “Correlations for the double-diffusive natural convection in square enclosures induced by opposite temperature and concentration gradients,” *Int. J. Heat Mass Tran*., vol. 81, pp. 811–819, 2015.

[43] A. Mohamad, R. Bennacer, and J. Azaiez, “Double diffusion natural convection in a rectangular enclosure filled with binary fluid saturated porous media: the effect of lateral aspect ratio,” *Phys. Fluids*, vol. 16, no. 1, pp. 184–199, 2004.

[44] M. Stern, “Collective instability of salt fingers,” *J. Fluid Mech*., vol. 35, no. 02, pp. 209–218, 1969.

[45] J. Holyer, “The stability of long, steady, two-dimensional salt fingers,” *J. Fluid Mech*., vol. 147, pp. 169–185, 1984.

[46] E. Kunze, “Limits on growing, finite-length salt fingers: A Richardson number constraint,” *J. Mar. Res*., vol. 45, no. 3, pp. 533–556, 1987.

[47] W. Merryfield, “Origin of thermohaline staircases,” *J. Phys. Oceanogr*., vol. 30, no. 5, pp. 1046–1068, 2000.

[48] T. Radko, “A mechanism for layer formation in a double-diffusive fluid,” *J. Fluid Mech*., vol. 497, pp. 365–380, 2003.

[49] B. Ruddick and O. Kerr, "Oceanic thermohaline intrusions: theory," *Prog. Oceanogr*., vol. 56, no. 3, pp. 483–497, 2003.

[50] K. Sreenivas, O. Singh, and J. Srinivasan, "On the relationship between finger width, velocity, and fluxes in thermohaline convection," *Phys. Fluids*, vol. 21, no. 2, pp. 026601(1)–(15), 2009.

[51] S. Stellmach, A. Traxler, P. Garaud, N. Brummell, and T. Radko, "Dynamics of fingering convection. part 2 the formation of thermohaline staircases," *J. Fluid Mech*., vol. 677, pp. 554–571, 2011.

[52] K. Sahu and O. Matar, "Stability of plane channel flow with viscous heating," *J. Fluids Eng*., vol. 132, no. 1, pp. 011202(1) – (7), 2010.

[53] W. Goux, L. Verkruyse, and S. Saltert, "The impact of Rayleigh-Benard convection on NMR pulsed- field-gradient diffusion measurements," *J. Magn. Reson*., vol. 88, no. 3, pp. 609–614, 1990. 30

[54] A. Boycott, "Sedimentation of blood corpuscles," *Nature*, vol. 104, p. 532, 1920.